Int J Earth Sci (Geol Rundsch) (2002) 91:698–711
DOI 10.1007/s00531-001-0244-9

ORIGINAL PAPER

Jens Greinert · Gerhard Bohrmann · Marcus Elvert

Stromatolitic fabric of authigenic carbonate crusts: result of anaerobic methane oxidation at cold seeps in 4,850 m water depth

Received: 21 December 2000 / Accepted: 19 November 2001 / Published online: 30 April 2002

Abstract Methane seepage leads to Mg-calcite and aragonite precipitation at a depth of 4,850 m on the Aleutian accretionary margin. Stromatolitic and oncoid growth structures imply encrustation of microorganisms (microbial mats) in the host sediment with a unique growth direction downward into the sediment, forming crust-shaped lithologies. Biomarker investigations of the residue after carbonate dissolution show strong enrichments in crocetane and archaeol, which contain extremely low $\delta^{13}C$ values. This indicates the presence of methane-consuming archaea, and $\delta^{13}C$ values of –42 to –51‰ PDB indicate that methane is the carbon source for the carbonate crusts. Thus, it appears that stromatolitic encrustations of methanotrophic anaerobic archaea probably occurs in a consortium with sulphate-reducing bacteria and that carbonate precipitation proceeds downward into the sediment, where ascending cold fluids provide a methane source. Strontium and oxygen isotope analyses as well as ^{14}C ages of the carbonates suggest that the fluids come from deep within the sediment and that carbonate precipitation began about 3,000 years ago.

Keywords Aleutian accretionary margin · Anaerobic methane oxidation · Archaea · Fluid seepage · Stromatolitic fabric

Introduction

Accretionary prisms are areas where dewatering of the sediment occurs because of sediment compaction, tectonic pressure and geochemical reactions of solid phases such as the decomposition of organic matter or clay mineral transformations (e.g. Kastner et al. 1991; Moore and Vrolijk 1992). Cold seeps occur where this excess water is released into the water column (e.g. Aharon 1994). Here, the ascent of reduced chemical species (dominantly methane and hydrogen sulphide) from deeper sediment horizons and different diagenetic zones result in both the colonization of the seep-area with anaerobic microorganisms (bacteria, archaea) and chemoautotrophic macroorganisms such as clams, Pogonophora or Vestimentifera. In addition, the mixing of pore water from different diagenetic zones causes geochemical reactions, which result in the formation of barite or carbonate precipitates (Ritger et al. 1987; Kulm and Suess 1990; Fu et al. 1994; Bohrmann et al. 1998; Nähr et al. 2000; Greinert et al. 2001a, 2001b). The generation of carbonates is a well-known feature for cold seep sites where methane is expelled from the seafloor. Carbonate precipitation is closely coupled with the oxidation of methane via sulphate reduction by a consortium of anaerobic archaea and bacteria, which release HCO_3^- into the pore and bottom water (Iversen and Jørgensen 1985; Han and Suess 1989; Masuzawa et al. 1992; Paull et al. 1992; Whiticar 1996). Isotopic analyses of the carbonate phases and the biomarkers demonstrate the incorporation of methane-derived carbon and elucidate the mechanism of the methane oxidation (Elvert et al. 2000; Boetius et al. 2000; Greinert et al. 2001a). Petrographic investigations provide more detailed information about the fabric-forming mechanisms and the ancient fluid-venting activity.

The general formation mechanism of stromatolitic carbonates is a process of binding fine sediment particles to microbial mats (e.g. bacteria, algae) together with a continuous encrustation by the precipitating of carbonate. The precipitation is induced by the fixation of CO_2 from seawater, sulphate reduction of organic matter, anaerobic sulphide oxidation and abiotic surface precipitation (Riding 1991; Rasmussen et al. 1993; Grotzinger and Rothmann 1996; Visscher et al. 1998; Knoll and Semikhativ 1998). In contrast to this, biological processes, such as aerobic respiration and aerobic sulphide oxidation, cause carbonate dissolution (Visscher et al.

J. Greinert (✉) · G. Bohrmann
GEOMAR Research Center for Marine Geosciences,
Wischhofstrasse 1-3, 24148 Kiel, Germany
e-mail: jgreinert@geomar.de

M. Elvert
Max-Planck-Institute for Marine Microbiology, Celsiusstrasse 1,
28359 Bremen, Germany

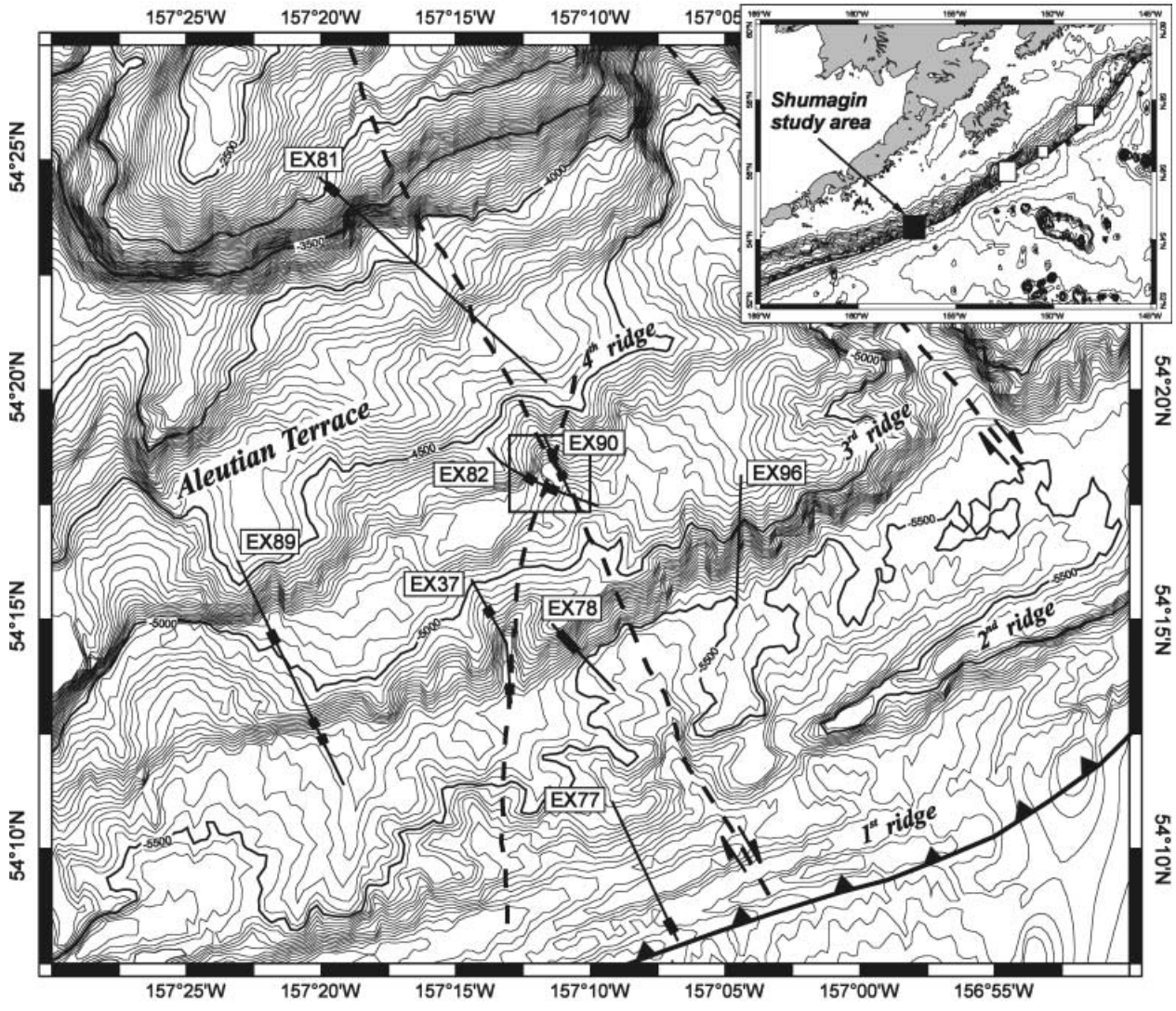

Fig. 1 Bathymetric map of the deeper part of the Aleutian accretionary prism at the Shumagin study area. *Lines labelled EX* represent TV-guided observation tracks; the broader parts mark areas where signs of fluid seepage were found. *Dashed lines* are possible dextral fault systems. *Line with triangles* shows the position of the deformation front. *Open boxes within the inset map* are other study areas with active fluid seepage (Suess et al. 1998)

1998). Because light is needed for photosynthesis of algae and structural analyses indicate influences of waves or small-scale changing sea levels, stromatolitic fabrics are generally thought to represent shallow water environments (Hofmann 1973; Feldmann and McKenzie 1998; Duane and Al-Zamel 1999). Nevertheless, the carbonate crusts presented here also show a stromatolitic fabric, even though they were formed at 4,850 m water depth. The mechanism and the particular geochemical environment that cause the authigenic formation of stromatolitic carbonates below the carbonate compensation depth (CCD) are the subject of this paper.

Geological setting of the Shumagin study area

The Aleutian margin is characterized by the subduction of the Pacific Plate under the North American Plate, with an active volcanic arc and accretionary prism. During RV *Sonne* cruises in 1994 (SO97) and 1996 (SO110) four different working areas between 148° and 157°W were studied (Fig. 1). These cruises documented living cold seep communities, authigenic barite and carbonate precipitation and methane anomalies in the water column. Furthermore, in-situ flow rates and geochemical compositions showed that active fluid seepage existed in all four areas (Suess 1994; Wallmann 1997; Suess and Bohrmann 1997; Suess et al. 1998).

At the westernmost Shumagin area, steep seaward-dipping flanks of the accretionary ridges constitute the dominant morphological feature (Fig. 1). These ridges are accreted from neogenic clastic material of the old Zodiac Fan deposits that overlie the oceanic crust and glacial sediments transported from the Aleutian peninsula. In addition to the normal sediment compactions, this accretion causes a sediment pore space reduction of 25

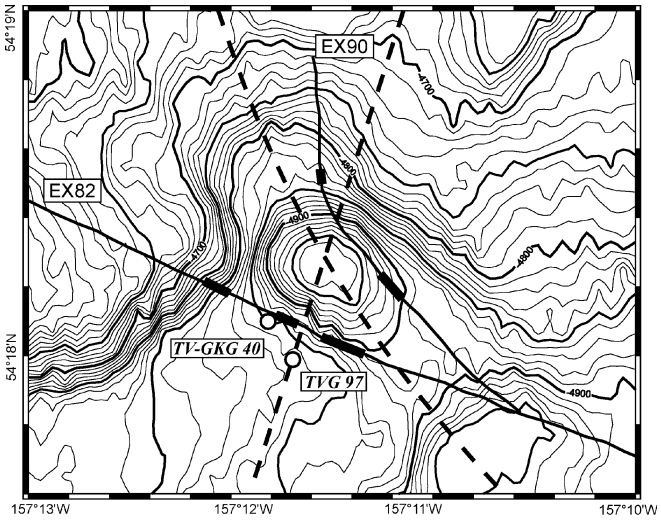

Fig. 2 Bathymetric map of a canyon structure at the fourth accretionary ridge where cold vent sites could be observed and authigenic carbonates were sampled (TVG 97 and TV-GKG 40). Meaning of lines see Fig. 1

and 50% within the three youngest ridges during the last 3 million years (von Huene 1989). This reduction is one of the major triggering factors for the advection of fluids and the formation of cold seeps on the seafloor.

Canyons that cut into the ridges are another morphological feature. The canyons are possibly induced by NNE–SSW-trending dextral strike-slip faults, which are typical for this part of the Shumagin segment along the Aleutian margin (Lewis et al. 1988). These deeply penetrating faults are ideally suited to serve as pathways to transport fluids from deep in the accretionary prism up to the seafloor.

Locations of vent activity were identified with the TV-guided camera sled Explos, which also recorded strong indications of fault-controlled active fluid seepage, especially at the seaward flanks of the ridges (Fig. 1). Typical indications of methane- and H_2S-rich fluid flow were fields of the white clam *Clayptogena phaseoliformis*, shells of *Acharax* spp., and Pogonophora. Pogonophora rim the *Clayptogena* fields, which have typical diameters of less than 2 m. At the Shumagin area, the population of the observed seep sites is much thinner in general than in the easternmost Edge area (Suess et al. 1998), but denser populations of *Claptogena* were found at a canyon-like structure on the fourth accretionary ridge (Figs. 1 and 2). Here, the sediment-covered seafloor also shows bacterial mats that are indicated either by lighter patches some decimetres in size or by lighter halos around slightly elevated sediment areas with a rough gravel-like appearance (Fig. 3). Sampling of these seep sites was performed using a TV-guided grab (TVG) and a TV-guided box corer (TV-GKG). Carbonate crusts were recovered at two stations (TVG 87/TV-GKG 40; Fig. 2). During the sampling at station TVG 97 the TV-grab fell over, which may have been caused by the steep morphology or by intensively cemented sediment that could not be penetrated by the TV-grab. Only carbonate crusts were recovered, no sediment was retrieved. The recovery of an undisturbed sediment sample would have provided pore water for analysis, providing evidence for the carbonate formation and the in-situ orientation of the carbonate crusts. The latter is important for understanding the unique crust formation described here.

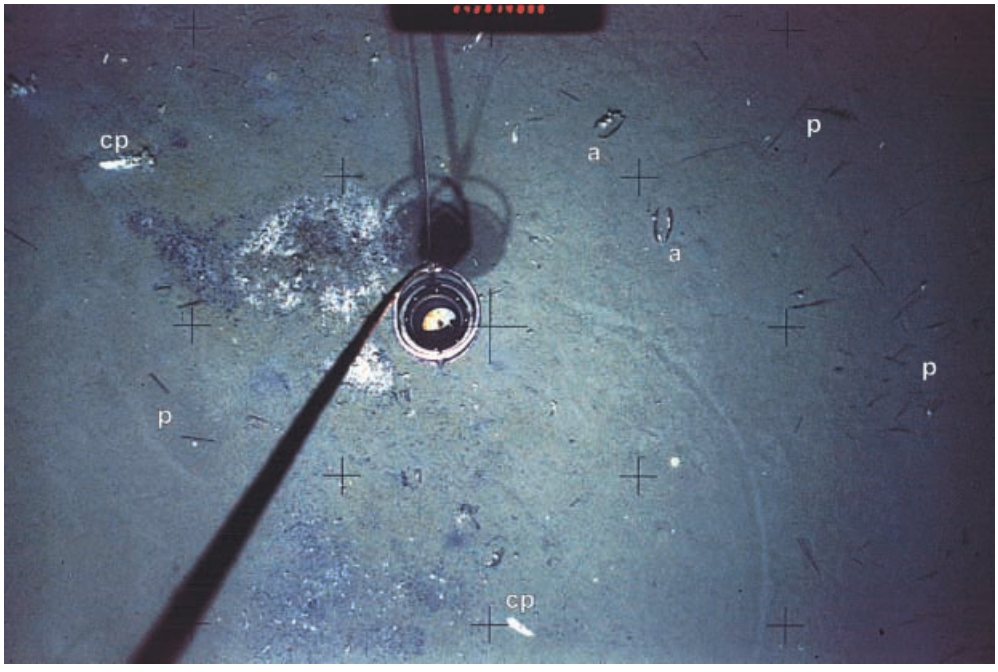

Fig. 3 Seep site at the seafloor similar to the areas sampled by TVG 97 and TV-GKG 40. The rough surface left of the compass very probably represents a carbonate cemented area surrounded by white bacteria mats. White clam shells are *Calyptogena phaseoliformis (c*p), dark shells are *Acharax* spp. *(a*), darker lines are Pogonophora *(*p) and their shadows. The diameter of the compass is ~20 cm

Analytical methods

Petrographic investigations included microscopic investigations of thin sections using polarized and UV light. Cathodoluminescence (CL) investigations (Technosyn 8200 MK II) were carried out at the Catholic University Leuven, Belgium. X-ray diffraction analyses (XRD) of powdered samples identified the cementing carbonate phases. This method also allowed a semi-quantitative estimation of the amount of high Mg-calcite (hMc) and aragonite (arag) based on the integrated peak areas of the (104) hMc and the (111) aragonite reflections (e.g. Milliman 1974; Greinert 1999). A scanning electron microscope (SEM; CamScan) equipped with an EDS X-ray microanalyser (Edax) was used for microanalyses.

For $\delta^{13}C$ and $\delta^{18}O$ isotope analyses the carbonates were carefully subsampled by a microdrill. Extraction of CO_2 for isotope measurements was performed using pure H_3PO_4 at 75 °C in a Carbo-Kiel online device connected to a Finnigan MAT 252 according to Wachter and Hayes (1985). Replicate analyses of a laboratory standard showed standard deviations better than 0.03‰ for $\delta^{18}O$ and 0.02‰ for $\delta^{13}C$. All C and O isotope data are given relative to PDB standard.

^{14}C-age determinations were provided by AMS analyses, Leibnitz Laboratory Kiel. The ages were corrected for ^{14}C fractionation using the $^{13}C/^{12}C$ isotope ratio. Samples were treated with H_2O_2 to remove organic material prior to the extraction of CO_2 with pure H_3PO_4 at 50 °C. Strontium isotope ratios were measured on acid leachates with a Finnigan MAT 262; strontium was separated on cation exchange columns with 2.5-N HCl and dried at 120–150 °C.

Lipid biomarkers were isolated from one carbonate crust at station TVG 97 by using 1 N HCl for carbonate dissolution. Procedures for the extraction of the residue after carbonate dissolution, the separation of the lipid extract and the gas chromatographic analyses are described by Elvert et al. (1999, 2000). Carbon isotope analyses of the biomarkers were performed by gas chromatography–combustion–isotope ratio mass spectrometry (GC-C-IRMS) using a Varian 3300 gas chromatograph interfaced to a Finnigan MAT 252 mass spectrometer at the University of Victoria, Canada. Analytical reproducibility of the complex mixtures was about ±1.6‰ PDB (Elvert et al. 2000).

Geochemical analyses of the carbonate phase were performed by ICP measurements. Bulk samples were ground and the carbonate phase was carefully dissolved in 1 N acetic acid several times to prevent a release of Mg, Fe and Mn from clay minerals or sulphides (Greinert 1999).

Results and discussion

Macroscopic and microscopic sample description

Carbonates recovered at station TVG 97 are crust-like precipitations of 50 to 200 mm in diameter and 5 to 70 mm in thickness. Their top and bottom sides are different in appearance (Fig. 4A1, A2). One side is wavy, smooth and strongly cemented, whereas the other one is rough and covered by uncemented to partly cemented sediment. The sediment of the TVG 97 crusts is densely penetrated by small holes (0.5–1 mm in diameter) spaced less than 4 mm apart (Fig. 4A1). *Acharax* shells are incorporated in one crust from station TVG 97, and they are still enclosed by an intact dark periostracum (Fig. 4A, F). Crusts from station TV-GKG 40 are generally smaller and strongly cemented, and both sides are irregular and rough (Fig. 4B). One side of the biggest crust from this station is covered by sediment and penetrated by holes: similar in size to those from station TVG 97. Small tubes of organic material were fixed to this crust side, and these tubes very probably originate from the tube worm Pogonophora (Fig. 4B1). Their diameter coincides with the diameter of the holes suggesting that the holes are casts of Pogonophora.

In cross cuts of samples from TVG 97 round to oval structures occur between the unconsolidated sediment and an area of thin stromatolitic laminae that forms the smooth sides of the crusts (Fig. 4C–F). The internal structure of the oval structures (3–15 mm in diameter) displays concentric thin layers that are light to dark grey in colour with an additional radial structure. Because their size, shape and internal structure correspond to oncoids, we will use this term in a descriptive sense for these oval structures. In contrast to oncoids that form in shallow water, a detrital nucleus could not be found in any of the oncoidal structures under investigation. Instead, open or rim-cemented pores of round to oval shape are frequently present in the centre of these oncoids. Some of the pores are completely cemented as well (Fig. 4C, F). The varying oval to round shape suggests that these pores are channels with a diameter that is equivalent to the holes in the uncemented sediment area of the crusts. It becomes clear that the holes in the sediment are worm channels that do not reach into the cemented laminae area. Various isolated oncoids show a thin rim as the beginning of a new layer that does not necessarily surround the oncoid completely. Typically, these rims occur on that oncoid side facing the smooth crust side (Fig. 4C, E). Frequently, the oncoids are enveloped by or even incorporated into the laminated area. This area is built of light grey to black laminae of 0.1 to 2.5 mm in thickness. They are interlaced with lightly coloured non-continuous layers 0.1 to 1 mm thick and several millimetres long (Fig. 4C–F). Some laminae overlap others, mainly black ones; the overlapping laminae always occur closer to the smooth crust side (Fig. 4D, F). In some places, a cloudy carbonate cementation occurs irregularly in the unconsolidated

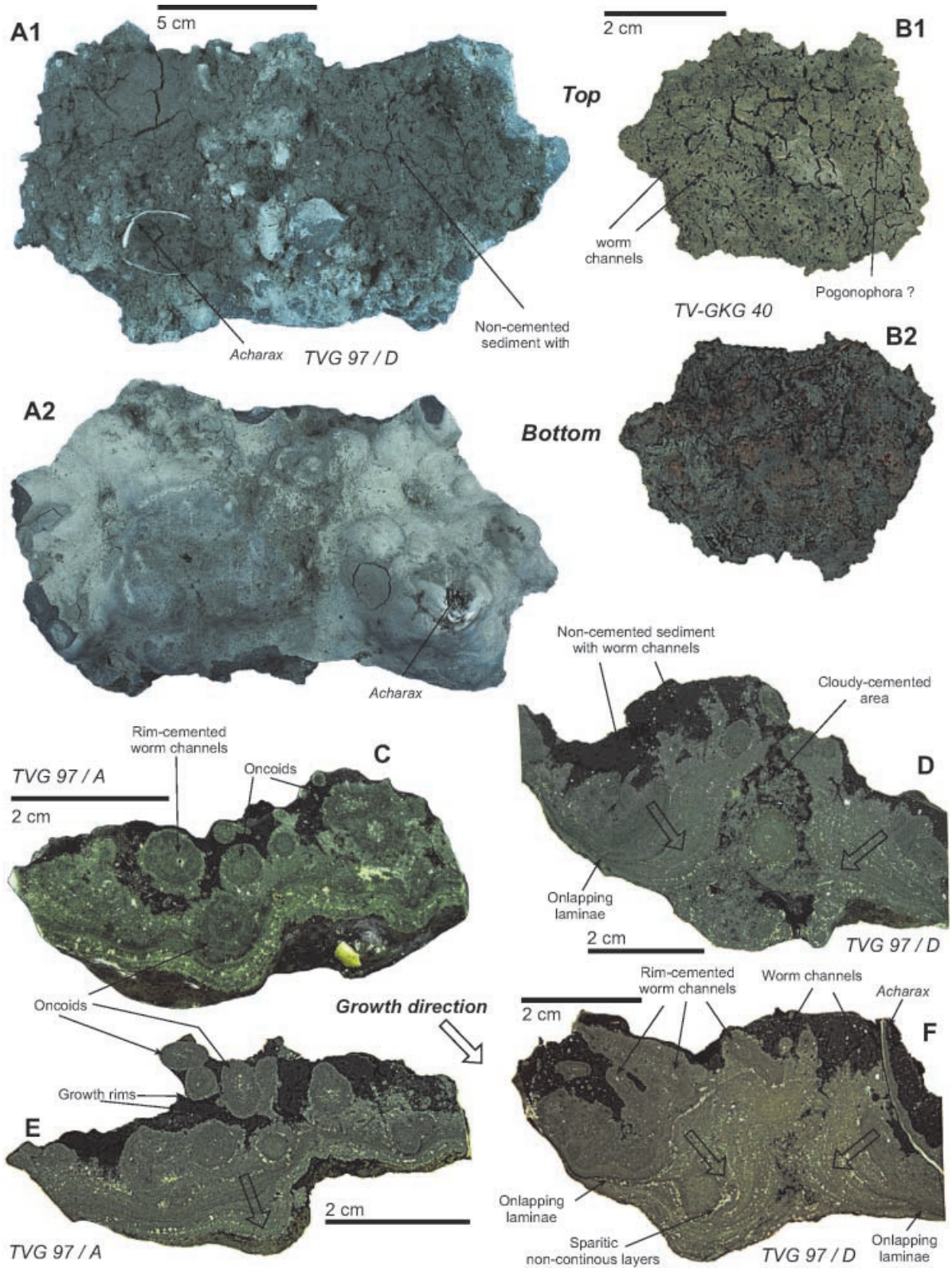

Fig. 4A–F Specimens and cross cuts of carbonate crusts from stations TVG 97 and TV-GKG 40. Samples from station TVG 97 have different morphologies on each side of the crust; a wavy, strong cemented side with a stromatolitic laminae structure (**A2**) and a rough crust side of uncemented sediment, which is densely penetrated by worm channels (**A1**, **B1**, **B2**). The stromatolitic laminae and their enveloping of round structures with oncoid fabric indicate a growth direction towards the smooth crust side and point to a biogenetically induced crust formation (**C**–**F**)

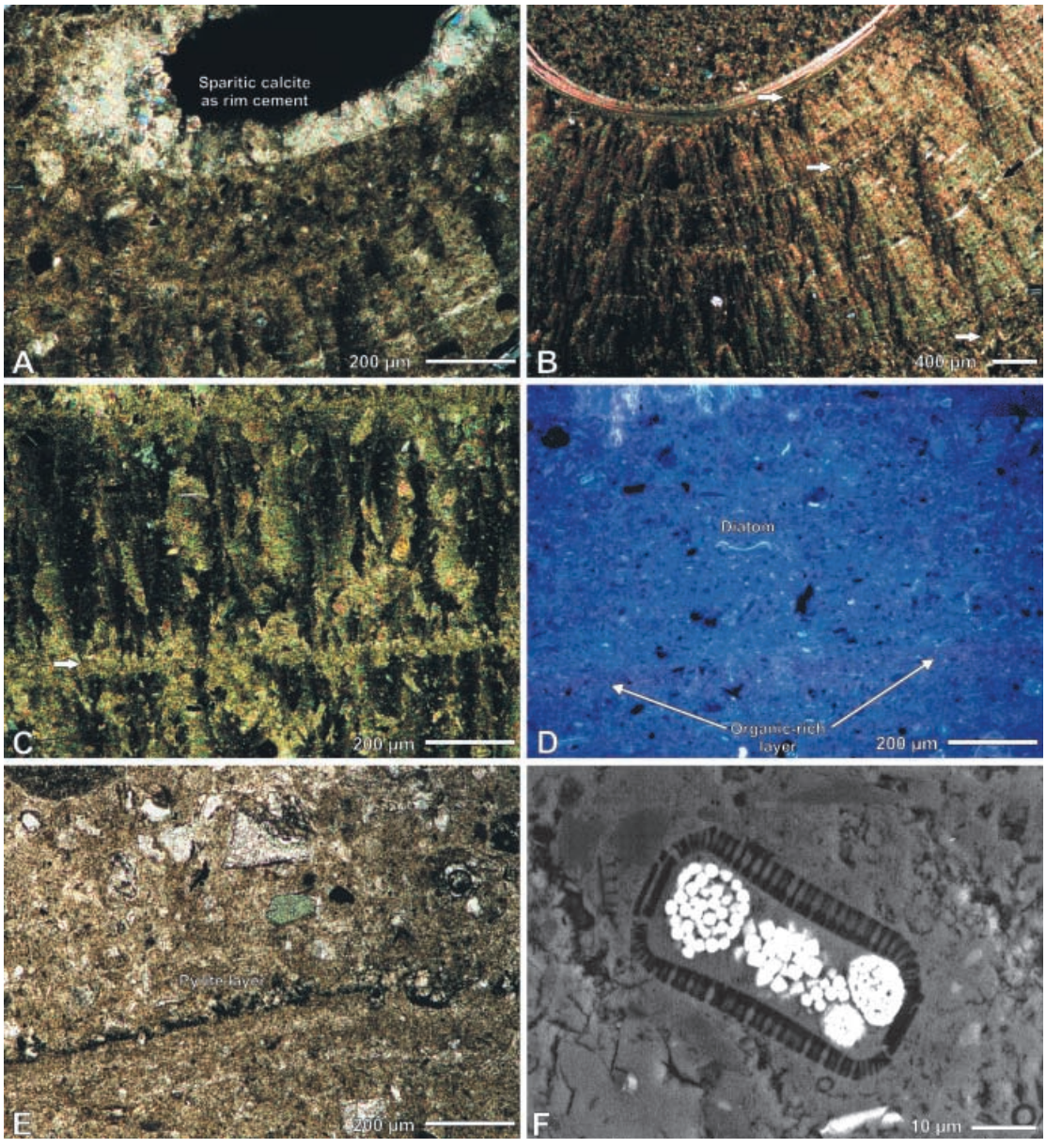

Fig. 5A–F Light and SEM microscopic images of carbonates from station TVG 97. **A–C** Crossed nicols; **D** UV-light; **E** parallel nicols, **F** SEM. **A–D** The mainly micritic sediment cementation with interlaced sparitic laminae. **A** shows sparitic calcite within a worm channel. **B** Laminae growing parallel to a clam shell surface are visible. Images in **C** and **D** show the same area; in **D** a reddish fluorescence layer just below the lighter laminae in **C** indicates higher amounts of organic matter. **E** Laminae parallel layer of idiomorphic pyrite crystals. **F** Framboidal pyrite in diatom shells indicates a formation in anoxic microenvironments within the frustals caused by the decomposition of the organic matter

sediment (Fig. 4D) or between oncoids and the laminated area.

Predominately, micritic calcite was found to be the carbonate cement in laminae, oncoids and the cloudy cemented areas. The macroscopically lighter laminae are more coarsely crystalline (microspar to sparite) with less or no impurities from the siliceous sediment matrix. This matrix is composed of silt to sand-sized quartz, amphibole and feldspar grains, vesicular glass fragments, radiolarian and diatom skeletons, as well as detrital clay minerals (Fig. 5A–D). Singular pyrite crystals or small pyrite clusters (together less than 5%) are randomly distributed or arranged in short, laminae-parallel layers (Fig. 5E). Clusters of framboidal pyrite were observed by SEM backscatter analyses in diatom frustals (Fig. 5F).

Differences between lighter and darker laminae, as well as between the oncoid-building layers, are produced by varying crystal sizes (which are rather homogenous in lateral direction) together with changing amounts of the siliceous matrix. Additionally, the amount of pyrite increases in the dark layers. Under crossed nicols, laminae and layers show a side-by-side fan-shaped sweeping extinction, which propagates from one point above a very thin micritic layer (Fig. 5B, C, white arrows). The fan

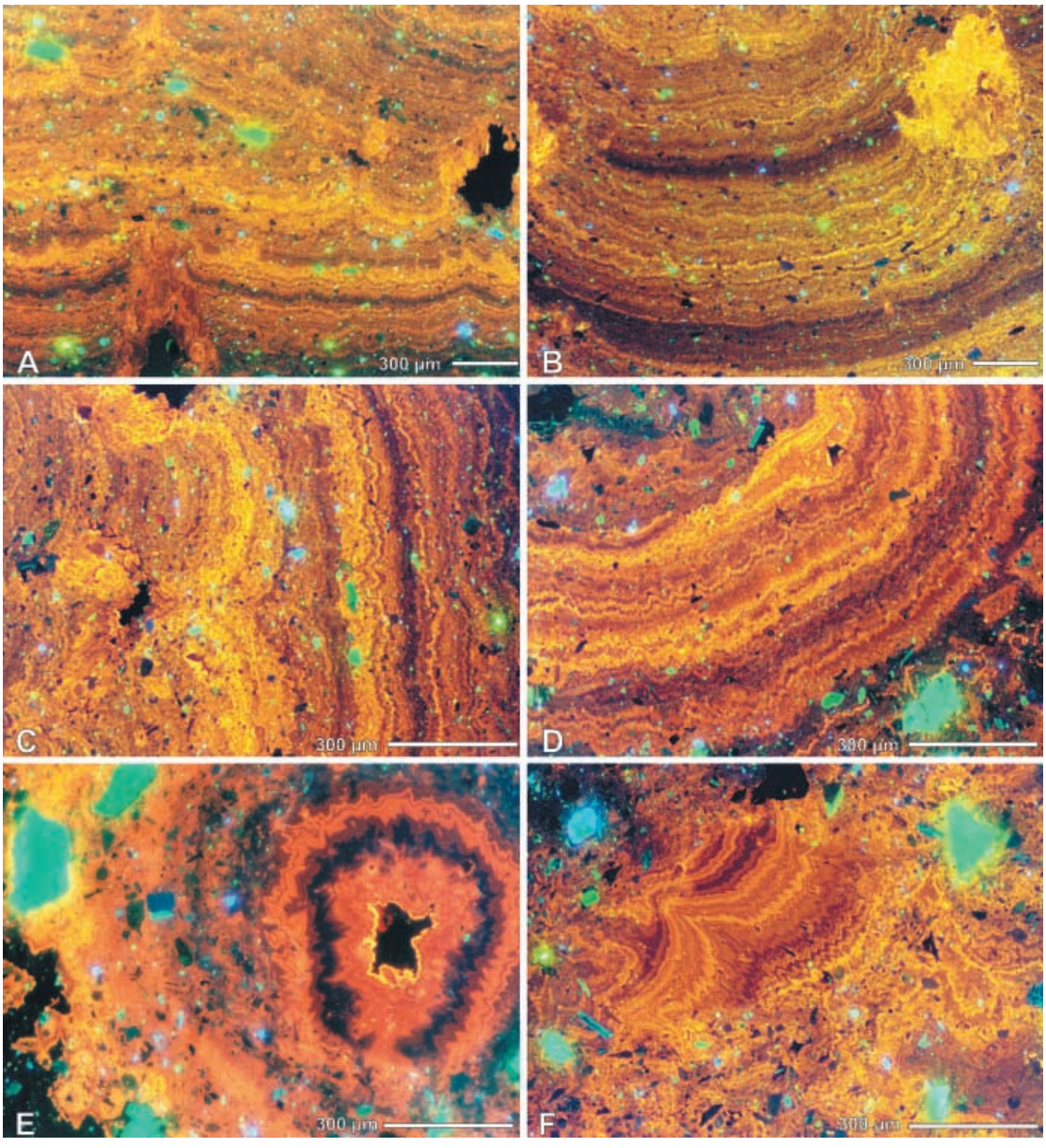

Fig. 6A–F CL microscopic images of carbonate crusts from station TVG 97. **A–D** Stromatolitic fabric of fine laminae that form columnar and domal growth structures; **C** is a close-up of **A** (rotated 90°). **E, F** Sparitic cements formed during different crystallization phases visible as a sequence of dark and light orange zones: **E** rim cement in a worm channel; **F** probably porphyroid recrystallization

propagation is terminated by the next thin micritic layer, but is unaffected by layers or lenses of coarser crystal size (Fig. 5B, black arrow). On clam shells, which do not show any signs of micritization, laminae occur only at the outer shell side with a subparallel orientation and a fan-like extinction rooted at the nearer-shell laminae side. In contrast, the area within the shells shows no lamination (Fig. 5B).

Indications of organic material are visible in UV-light, as shown by laminae-parallel reddish fluorescent layers (Fig. 5D). Under CL, a sequence of light orange to almost non-luminescent layers (10–100 µm in thickness) can be distinguished in both the laminae and oncoids (Fig. 6A–D) as well as in the sparitic rim cements of channels and other sparitic areas (Fig. 6E, F). The sharp change in colour and the colours themselves indicate abrupt varying amounts of Fe and Mn in the carbonate phase (Machel and Burton 1991). Most significant are wavy laminae patterns similar to the cauliflower-like structures of stromatolites in which domal laminae overlay separately growing columnar structures (Fig. 6A, C). Typically, the domal laminae are closer to the smooth crust side.

The occurrence of oncoid-like forms and wavy laminae that grow parallel to existing surfaces and their enveloping of oncoids indicate that carbonate formation is induced by the encrustation of microbial mats. In particular, the detection of laminae under CL is strong evi-

dence for stromatolitic crust growth (Adams et al. 1986; Burne and Moore 1987; Southgate 1989; Riding 1991; Zhang et al. 1993). Unfortunately, relics of microorganisms could not be found in either the thin sections or by SEM investigations of carefully acid-treated samples. Nevertheless, the laminae-parallel accumulation of organic matter strengthens the assumption of stromatolitic crust formation by carbonate-forming microorganisms.

Varying luminescence of laminae, oncoid layers and sparitic cements corresponds to a temporal sequence of geochemical conditions during their formation. These conditions may oscillate between suboxic and anoxic, where dissolved Mn and Fe respectively are released into the pore water. The incorporation of changing amounts of Fe and Mn into the carbonate lattice results in different colours in CL investigations (Walker and Burley 1991). Clusters and layers of pyrite provide evidence of anoxic pore water conditions. Pyrite formation in general changes the Fe-concentration of the pore water and may be an important mechanism in exclusively anoxic conditions for lessening the incorporation of Fe in the calcite lattice and causes a bright yellow luminescence in CL.

Evidence for the growth direction of the crusts is provided by the relationship of the oncoids and the laminated area. The enveloping and the incorporation of oncoids by laminae indicate that the oncoids grew first. The laminae, which are overlapped by those laminae nearer to the smooth crust side, clearly support a crust propagation towards the smooth crust side (Fig. 4). Incorporated *Acharax* shells and open channels of Pogonophora casts indicate a crust formation near/at the sediment surface. Seafloor observations revealed that seep sites are characterized by rough sediment surfaces (Fig. 3). Taking this and the open Pogonophara casts (the open channels in the uncemented sediment) into account we propose that the smooth side is the bottom side of the crust.

Mineralogy and carbonate content

XRD analyses of the carbonate crusts from station TVG 97 were used to identify detrital minerals of the host sediment such as quartz, feldspar, amphibole and the clay minerals chlorite and illite. Mg-calcite with 7 mol% $MgCO_3$ is the dominant carbonate phase. In only one sample aragonite was identified as a minor component. SEM-EDX investigations demonstrate that the rim cements within the worm channels are stoichiometric calcite. Geochemical analyses of the carbonate phase reveal that Fe (0.07–0.1 mol%) and Mn (0.03 to 0.04 mol%) are present (Greinert 1999), which are crucial for the characteristic CL patterns. The crusts from TV-GKG 40 also contain Mg-calcite (6 mol% $MgCO_3$), but they have a higher content of aragonite (up to 88 wt%, Table 1). The detrital components in TV-GKG 40 carbonates are identical to those of TVG 97 samples.

Porphyroid recrystallization of aragonite (or micrite) might be the reason for the microspar to sparite layers and lenses, which do not terminate laminae showing fans of sweeping extinction (Fig. 5B, black arrow). However, taking into account recently presented results (Kendall and Iannace 2001), we suggest that recrystallization can be neglected as an important process in our samples. A detailed discussion of the reasons for this would lead too far within the framework of this article.

Table 1 Carbonate mineralogical and isotopic analyses of carbonate subsamples from station TV-GKG 40

Aragonite (wt%)	Calcite (wt%)	δ^{18}O‰ PDB	δ^{13}C‰ PDB
6	94	2.95	–49.16
38	61	2.90	–45.63
88	12	3.36	–44.01
–	–	3.43	–44.24
40	60	2.85	–49.40
45	55	3.08	–47.87
–	–	2.88	–42.70
–	–	2.88	–42.94
–	–	2.83	–42.94

The carbonate contents were determined in different laminae of the samples from TVG 97 and these contents vary from 43 to 48 wt%. Compared with the general pore volume of marine surface sediments, a more or less complete carbonate cementation of the intergranular pore space can be suggested for our samples. No trend in carbonate content across the crusts or within oncoids was observed.

Carbon and oxygen isotopes

In order to identify the carbon source and the carbonate-forming mechanism, carbon isotope analyses were carried out on the same subsamples, which were also analysed mineralogically. Also, a shell of an *Acharax* specimen was analysed (Table 2). Carbon isotope values range from –50.83 to –47.02‰ δ^{13}C in TVG 97 samples and are similar in crusts from TV-GKG 40 (–49.90 to –42.70‰ δ^{13}C). These values unambiguously indicate that methane is the major carbon source of the carbonates at stations TVG 97 and TV-GKG 40 (Ritger et al. 1987; Han and Suess 1989; Kulm and Suess 1990; Masuzawa et al. 1992; Paull et al. 1992; Greinert et al. 2001a). In contrast, the carbon isotope values of the clam shell are much higher (–1.83 to –6.50‰; Table 2; Fig. 7), suggesting its carbon comes mainly from a source other than methane.

Biomarker investigations

Gas chromatographic analysis of the hydrocarbons obtained from a dissolved carbonate crust fragment from station TVG 97 show a predominance of the irregular isoprenoid crocetane (Fig. 8). Based on molecular and isotopic evidence, this biomarker has been previously identified to be from archaea involved in the anaerobic

Table 2 Isotopic analyses from TVG 97. Crust samples are Mg-calcite with 7 mol% $MgCO_3$. *Acharax* samples are pure calcite

Samples	$\delta^{18}O$‰ PDB	$\delta^{13}C$‰ PDB
Carbonate crust	2.62	–50.83
	2.57	–49.54
	2.37	–50.01
	2.11	–48.46
	2.53	–47.56
	2.51	–50.35
	2.46	–48.70
	2.40	–48.17
	2.41	–48.73
	2.42	–48.17
	2.18	–47.78
	2.36	–46.90
	2.41	–49.74
	2.40	–47.52
	2.59	–47.90
	2.48	–47.02
	3.23	–48.23
	2.53	–48.45
	2.58	–45.96
	2.58	–48.45
	2.48	–50.36
	2.41	–50.20
	2.47	–50.73
Acharax shell	3.60	–6.50
	3.50	–3.59
	3.45	–2.71
	3.49	–3.09
	3.61	–5.08
	3.70	–2.41
	3.54	–1.83
	3.53	–2.36
	3.62	–5.11

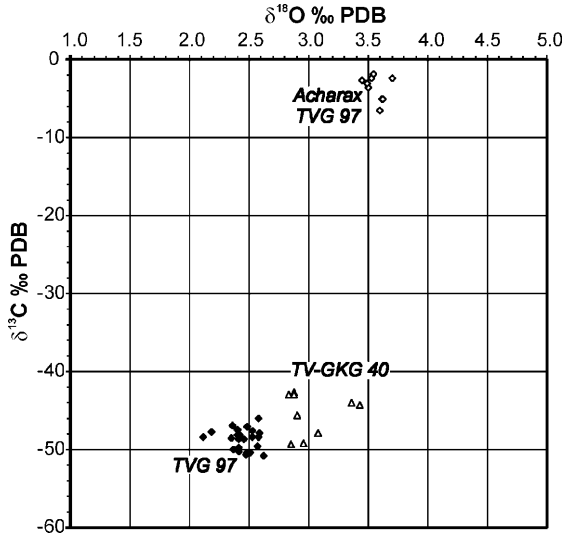

Fig. 7 $\delta^{13}C$ versus $\delta^{18}O$ diagram of carbonate crust and clam samples recovered from stations TVG 97 and TV-GKG 40

oxidation of methane (Elvert et al. 1999; Thiel et al. 1999; Elvert et al. 2000). Moreover, Elvert et al. (2000) detected the biomarker archaeol as the dominant compound in the respective alcohol fraction. Archaeol is

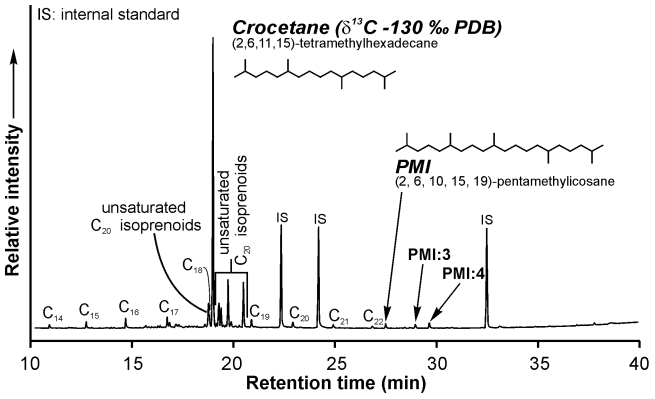

Fig. 8 Gas chromatogram of the hydrocarbon fraction obtained from a Mg-calcitic sample at station TVG 97. n-alkanes are marked by their number of carbon atoms. The biomarker crocetane, with a $\delta^{13}C$ value of about –130‰, indicates the presence of methanotrophic archaea

known to be one of the most common ether lipids in archaea (de Rosa and Gambacorta 1986). Both biomarkers, crocetane and archaeol, exhibited carbon isotope values highly depleted in ^{13}C (–130 and –124‰, respectively). Similar biomarkers were found in the sediment from TV-GKG 40, providing strong evidence that methane-consuming archaea are common at the sampled cold seep sites in the Shumagin area. Pore water analyses at station TV-GKG 40 also show a strong sulphate reduction with only 5 mM SO_4^{2-} at 5 cm sediment depth (Elvert et al. 2000), which points to recent sulphate reduction.

Carbonate formation induced by anaerobic methanotrophy

The presence of archaeol biomarkers with low $\delta^{13}C$ values and the significantly low $\delta^{13}C$ carbonate values strongly indicate that methanotrophic archaea induced carbonate precipitation. But carbonate formation via methane oxidation at cold seeps is typically coupled with bacterial sulphate reduction, which consumes hydrogen that was generated by methane-oxidizing archaea (Hoehler et al. 1994; Elvert et al. 1999; Thiel et al. 1999; Pancost et al. 2000). Biomarkers of sulphate reducers were not found, but the pore water analyses at TV-GKG 40 (Elvert et al. 2000) and the occurrence of laminae-parallel pyrite layers (precipitating from HS^- probably released during sulphate reduction and dissolved Fe^{2+} of the pore water; Fig. 5E) indicate sulphate reduction.

Because of the need of sulphate as well as methane, formation of methane-derived carbonates at cold seeps typically occurs in a distinct environment that has neither purely oxidizing nor purely reducing conditions. These conditions are present at the base of the sulphate reduction zone in transition to the methanogenic zone where methane is supplied by fluids (Kulm et al. 1986; Ritger et al. 1987; Suess and Whiticar 1989; Kulm and Suess 1990; Paull et al. 1992; von Rad et al. 1996;

Savard et al. 1996; Visscher et al. 1998). The encrustation of the clam shells, the worm channels in uncemented sediment and the strong decrease of SO_4^{2-} in the pore water of TV-GKG 40 (Elvert et al. 2000) suggest that carbonate crust formation very likely occurred close to the sediment surface. Accordingly, the base of the sulphate reduction zone must be close below the sediment surface because of the escaping geochemically reduced fluids.

Expulsion of biogenic methane

Evidence of methane advection by fluids was also obtained from direct CH_4 measurements in the water column. In the vicinity of stations TVG 97 and TV-GKG 40, CH_4 concentrations of up to 55 nl/l were analysed between 4,600 and 4,900 m water depth (Suess 1994), in contrast to a background concentration of around 10 nl/l in surrounding deep water. These high concentrations indicate a recently active expulsion of methane-rich fluids and confirm methane as a potential carbon source.

Two general mechanisms generate methane in the marine environment: biogenic methane formed via CO_2-reduction and thermogenic-methane generated during organic matter maturation (e.g. Whiticar 1996). Biogenic and thermogenic methane differ in their carbon and hydrogen isotopic composition and can be distinguished (Whiticar 1996). The measured $\delta^{13}C$ values of the carbonate crusts do not identify one of these mechanisms unambiguously. Carbon isotope values between –50.83 and –42.70‰ $\delta^{13}C$ represent a transition range of these both processes. Gas subsamples extracted from a sediment coated crust from TVG 97 (Suess 1994) yield methane concentrations of up to 13,600 ng/g (wet weight), but no higher hydrocarbons were detected. Maturation of organic matter generally releases higher hydrocarbons (Whiticar 1996) and their non-occurrence strongly indicates a biogenic methane origin.

Mixing of different carbon sources

With respect to $\delta^{13}C$ values of biogenic methane (generally lower than –60‰; Whiticar 1996), an admixture of at least one additional carbon source is needed to obtain the measured $\delta^{13}C$ values of the carbonate crusts (–42.7 to –50.8‰). Mixing also has to be assumed because pore water sulphate is needed for the methane oxidation process, as methane-containing fluids derived from the methanogenic zone are sulphate-free.

The most likely second carbon source is HCO_3^- released by the biogenic consumption of organic matter via sulphate reduction within the sulphate-reduction zone (e.g. Paull et al. 1992; Visscher et al. 1998). This released HCO_3^- has the same isotopic composition as marine organic matter and ranges from –15 to –25‰ $\delta^{13}C$ (Hoefs 1987). Assuming $\delta^{13}C$ values of HCO_3^- derived from methane (–60 ‰) and decomposed organic matter (–20 ‰), the amount of methane-derived carbon within the carbonate crusts can be estimated and varies between 57 and 77% (Appendix, note 1). Carbon species of the bottom water (North Pacific $\delta^{13}C_{\Sigma CO2} \approx 0.0$‰ PDB; Kroopnick 1985) are potentially an additional carbon source. Because most fluid-transported methane is oxidized at the base of the sulphate-reduction zone, a carbon source from the carbonate-dissolving bottom water seems less likely than carbon released by the carbonate-forming process of anaerobic organic matter decomposition.

Methane-derived carbon may be incorporated in the clam shells as well. In comparison to typical non-biogenic deep-water carbonates (Füchtbauer 1988), the clam $\delta^{13}C$ values (–1.83 to –6.50‰) are too low to be precipitated from North Pacific bottom water. The ^{13}C-depleted values are possible caused by the vital effects of the clams with a preferential incorporation of ^{12}C during shell development (Wefer and Berger 1991). Such vital effects can result in a comparable ^{13}C-depletion of –1 to –5‰ relatively to other bivalves (Hoefs 1987). Nevertheless, a mixture of bottom water ($\delta^{13}C$=0.0‰ PDB) and methane-influenced fluids is also a reasonable carbon source of the shell. The fluids may be assumed to have a $\delta^{13}C$ value corresponding to the carbonate crust growing near the surface (–41‰). Bottom water, thus, has to be mixed with 4 to 13% of the expulsing fluid water (Appendix, note 2) to produce the $\delta^{13}C$ values of the clam shells.

Age estimation of crust origin

The mixing of different carbon sources also influences the age estimation of the carbonate crusts. ^{14}C-analyses were performed on subsamples from edge of the smooth bottom-side of one crust and on an *Acharax* shell, both from station TVG 97 (Fig. 4A). Whereas the crust yielded an age of 19,270 years B.P. ±160 years, the shell was determined to be 5,840 years B.P. ±35 years. Because the *Acharax* clam was surely dead before it became cemented in the carbonate crust, the measured ^{14}C-age of this crust is not its formation age. Furthermore, the formation age cannot be older than the age of the clam shell minus the ^{14}C-age of North Pacific bottom water, which is 1,977 years (calculated from $\Delta^{14}C$=–212.7‰ at GEOSECS station 218 in 4,982 m water depth; Ostlund and Stuiver 1980). Thus, the crust had to have grown during the last 3,863 years. Even this age is still too old if an admixture of 4 to 13% seep-fluid to the bottom water is considered. A mixture of 90% bottom water (age 1,977 years) and 10% fluid with no ^{14}C activity would have a ^{14}C-age of around 2,847 years. Subtraction of this ^{14}C water age from the measured ^{14}C age of the clam then gives the true age of the clam of around 2,993 years. Consequently, the formation of the crust had to occur after that.

Stromatolitic crust growth into the sediment: ‘upside down’ carbonates?

From the geochemical and isotopic investigations it appears that crust formation at station TVG 97 is most likely caused by anaerobic oxidation of methane at a cold seep site. The similarity of the carbonate crusts to shallow water stromatolites and oncoids suggests an equivalent microbially mediated formation process. Usually, the growth direction of shallow water stromatolites proceeds exclusively into the water column (Füchtbauer 1988; Feldmann and McKenzie 1998; Knoll and Semikhatov 1998). A crust formation caused by carbonate over-saturation in the water column as a formation process can be excluded for the samples described here because both sampling sites are below the CCD.

It appears that the cold seep carbonates found at the Shumagin area are unusual ‘upside down’ carbonates growing downward into the sediment. Neumann et al. (1988) and Paull et al. (1992) already described ‘upside down’ carbonate crusts from methane vents on the Florida escarpment. Analogous to the crusts described here, the upper sides of the Florida crusts show irregular structures whereas the bottom sides are astonishingly smooth. This was interpreted to result from carbonate crystallization controlled by the flux of methane-enriched fluids and methane oxidation at the bottom sides of the crusts.

A similar formation can be assumed for the carbonate crusts described here. Oncoids grew in sediment horizons where both sulphate and methane occur simultaneously. Starting their formation around worm tubes and other potential substrates for the presumed syntrophic consortium of archaea and bacteria. Anaerobic decomposition of organic matter takes place at the same time producing additional HCO_3^-, which also contributes to carbonate precipitation. The concentric spreading occurs because of the unlimited propagation of encrusting microorganisms in the sediment without a space-limitation by previously grown structures. These microbial mats of archaea–bacteria also settle on clam shells and cause carbonate precipitation parallel to the shells. Triggered by the methane supply and the self-induced carbonate encrustation, the laminae forming microorganisms ‘move’ towards the methane as the ascending nutrition source. As cementation continues, oncoids and stromatolitic structures become surrounded by new microorganism laminae that build carpet-like colonies on the bottom side of the crusts (Fig. 4C, E). Carbonate encrustations of this layer constitute a barrier for ascending methane; thus additional microorganisms and carbonate laminae form towards the source of the methane, and consequently grow into the sediment towards the smooth crust side. Seafloor observations of slightly elevated rough sediment areas (Fig. 3) support the conclusion that the rough crust side is on top and indicate a downwardly directed crust propagation.

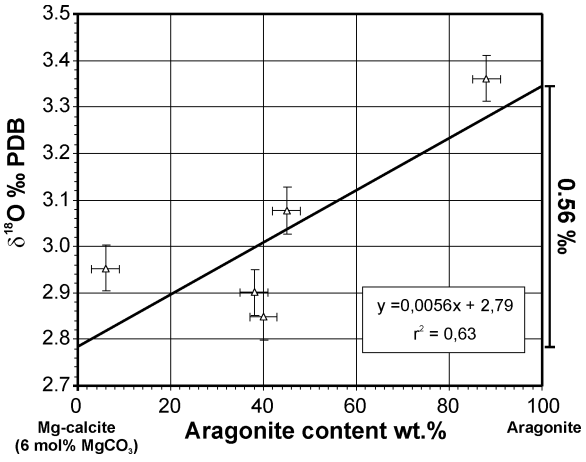

Fig. 9 Correlation between $\delta^{18}O$ values and the aragonite content in samples from station TV-GKG 40. The $\delta^{18}O$ values become higher with increasing aragonite contents because of differential ^{18}O fractionation between calcite and aragonite

Oxygen isotopes impacted by ^{18}O-depleted pore water

Analyses of $\delta^{18}O$ values of carbonates from TVG 97 vary between 2.11 to 2.62‰ whereas TV-GKG 40 samples show higher values from 2.83 to 3.43‰. The clam shell is even more enriched in ^{18}O showing values up to 3.70‰ (Table 2; Fig. 7).

To investigate whether the analysed $\delta^{18}O$ isotope values of the carbonate crusts reflect equilibrium crystallization, the relationships given by Friedman and O’Neil (1977) and Hudson and Anderson (1989) were used (Appendix, note 3). With a measured in-situ bottom water temperature of 1.62 °C (Suess and Bohrmann 1997) and an assumed $\delta^{18}O$ value for the pore water of 0.2‰ SMOW (after Hoefs’ 1987; the relationship between $\delta^{18}O$ in the North Pacific and salinity, here 34.65 psu), an equilibrium $\delta^{18}O$ value of 3.7‰ for calcite results. This value is identical to the measured values of the clam shell, which consequently might have formed in equilibrium with the bottom water. In contrast, the oxygen isotope data of the Mg-calcite from TVG 97 reveal that precipitation did not occur in equilibrium to a water of 0.2‰ show.

Similar conclusions can be drawn from the data of station TV-GKG 40. Here, oxygen isotope values are higher relative to station TVG 97. This can be explained by the higher aragonite content (Table 1). Figure 9 shows a linear correlation between increasing $\delta^{18}O$ values and an increasing amount of aragonite. Compared with a hypothetically Mg-calcite phase with 6 mol% $MgCO_3$, aragonite is enriched in ^{18}O by 0.56‰ (Fig. 9). If a correction for the larger fractionation of Mg-calcite relative to calcite is applied (0.06‰ per mol $MgCO_3$; Tarutani et al. 1969), the difference between an assumed aragonite and the Mg-corrected calcite increases to 0.92‰. This difference almost corresponds to the difference in fractionation that occurs during the formation of aragonite and calcite at cold temperatures (Tarutani et al. 1969; Kim and O’Neil

1997; Greinert 1999). The deviations of $\delta^{18}O$ values in carbonate crusts from stations TVG 97 and TV-GKG 40, therefore, are related to the respective mineral compositions and to the different fractionation processes associated with the formation of aragonite and Mg-calcite.

To explain the $\delta^{18}O$ values of the carbonates crusts from both stations, assuming equilibrium crystallization in pore water with 0.2‰ SMOW, the temperatures at stations TVG 97 and TV-GKG 40 should be 6.9 and 5.2 °C, respectively. Such high temperatures are unlikely in 5,000-m water depths compared to the measured in-situ bottom water temperature. At 1.62 °C, the pore water composition at station TVG 97 should range from –1.34 to –1.85‰ SMOW to produce the $\delta^{18}O$ value of the analysed Mg-calcite (Friedman and O'Neil 1977). A hypothetically pure aragonite sample of station TV-GKG 40 (3.35‰ $\delta^{18}O$, calculated from Fig. 9) also indicates a significant lower $\delta^{18}O$ pore water value of –0.81‰ SMOW (Hudson and Anderson 1989). Thus, we suggest ^{18}O-depleted source water is responsible for the recorded $\delta^{18}O$ values of the carbonate crusts.

Sr isotopes: evidence of rock–water interactions and deep-derived fluids

Sr isotope ratios of bulk samples of crusts from station TVG 97 may elucidate the reasons for the ^{18}O-depleted pore water near the sediment surface. The $^{87}Sr/^{86}Sr$ values vary between 0.708489 and 0.708336 and are significantly lower than the recent seawater value of 0.709175 (Paytan et al. 1993). The values correspond to Sr isotope value of a 21-Ma old seawater. It is probably true that old fluids are one source for these Sr-values but rock–water interactions between the ascending fluid and sediment components such as volcanic glass fragments, old carbonate horizons or even the subducted oceanic crust have to be considered as well.

In particular, the diagenetic transformation of volcanic glass to clay minerals releases strontium with low Sr-isotope values (Kay et al. 1978). Simultaneously, the pore water will be enriched in ^{16}O because heavy oxygen isotopes are bound preferentially into clay minerals as interlayer water (Gieskes and Lawrence 1981). This general process of ^{18}O incorporation in diagenetically formed minerals causes a successive ^{18}O-depletion in the pore water with increasing sediment depth (Hoefs 1987; Kastner et al. 1995).

Bruns et al. (1987) described an Oligocene carbonate horizon that occurs on top of the subducted sediments of the Zodiac Fan, directly below the accretionary complex of the Shumagin sector (Creager et al. 1973). Dissolution of this nanofossil-rich horizon ($^{87}Sr/^{86}Sr$ <0.70826) and the advection of the pore water would transport this low $^{87}Sr/^{86}Sr$ ratio into higher sediment horizons. Apart from that, an interaction between ascending fluids and the oceanic crust at only 3 km depth (Bruns et al. 1987) could modify the Sr isotope value of these fluids that transport ^{18}O-depleted pore water up to the sediment surface (Elderfield et al. 1990). Although the assumption of deep-derived fluids cannot be proved, the fault-controlled tectonic situation in accretionary prisms in general and the possible crossing of two fracture zones at the sampling area (Fig. 1) provide favourable conditions for deep-derived fluids escaping at the sampled cold seep sites.

Conclusion

Carbon isotope and biomarker investigations of carbonate crusts from two cold seep sites at the Aleutian accretionary margin show that carbonate precipitation is controlled by anaerobic methane oxidation of archaea. As indicated by pyrite layers and rapidly decreasing sulphate concentrations in the pore water, methane oxidation is linked to sulphate reduction. Thus, methane-oxidizing archaea and sulphate-reducing bacteria appear to initiate a carbonate precipitation in 4,850 m water depth within the sediment. This precipitation is probably younger than 3,000 years, which is the ^{14}C-age of a clam shell corrected for the ^{14}C-age of the North Pacific deep water and the contribution of methane in the clam carbon. Low oxygen isotope values of the carbonate phases, Mg-calcite and aragonite, as well as Sr isotope analyses, indicate that the fluids may be generated in deeper sediment horizons. Here, either rock–water interaction with the oceanic crust, an Oligocene carbonate horizon or volcanic glass influences the Sr composition of the generally ^{18}O-depleted pore water that migrates through the methanogenic zone and escapes as methane-rich fluid at the sediment surface.

The stromatolitic and oncoid structures of the carbonate crusts suggest an encrustation of microorganism laminae (microbial mats), which probably consisted of an archaea–bacteria consortium. The enveloping and incorporation of oncoids by stromatolitic laminae as well as the sequences of these laminae themselves indicate a crust growth propagating towards the smooth laminae-composed crust side. This smooth crust-side appears to be the bottom side of the crust because the opposite rough side being composed of uncemented sediment densely penetrated by open worm channels, is similar to the seafloor surface at the sampled seep sites. Laminae growth started when oncoid structures induced the development of microbial mats (laminae) that underlay and surrounded the oncoids from below. The encrustation of the first underlying and horizontally spreading laminae causes a downward growth of additional laminae into the sediment towards the ascending methane, which is the carbon source for methane oxidizing archaea. This crustal growth scenario results in 'upside down'-oriented stromatolitic carbonates and represents a microbially induced carbonate formation unique at cold seeps in 4.850-m water depth and may be of significance for the facies interpretation of similar structures in the fossil record.

Acknowledgements This paper contains parts of a PhD thesis of J.G. and M.E. The authors thank the crew of RV *Sonne* for providing professional help during the cruises SO97 and SO110. Further, we would like to thank Rudy Swennen from the Catholic University in Leuven (Belgium) for his help with CL investigations. We are grateful to B. Domeyer, J. Heinze and A. Bleyer, for help with mineralogical and geochemical analyses. For isotopic analyses, we would like to thank M. Joachimski (University of Erlangen) and M.J. Whiticar (University of Victoria). Thanks to E. Hütten, S. Gulick, R. Keir and J. Reijmer for useful discussions. M.E. was a member of the graduate school 'Dynamics of Global Cycles within the System Earth' supported by grants from the Deutsche Forschungsgemeinschaft (grant Schm 250/49) and the Land Schleswig-Holstein. Additional financial support was provided by the Federal Ministry of Education and Research, Bonn through grants 03G0097A and 03G0110B.

Appendix

1. Calculation of the amount of methane-derived carbon ($c_{methane}$) mixed with carbon from degraded organic matter to create a pore water $\delta^{13}C$ value that is conserved in the carbonate crusts:

   $$c_{methane}=(\delta^{13}C_{carbonate}-\delta^{13}C_{organic\ matter})/(\delta^{13}C_{methane}-\delta^{13}C_{organic\ matter})$$

2. Simplified mixing equation for calculating the amount of admixed fluid water (x) into the bottom water:

   $$\delta^{13}C_{seep\text{-}bottom\ water}= x \cdot \delta^{13}C_{fluid}+(1-x) \cdot \delta^{13}C_{normal\text{-}bottom\ water}$$

3. Oxygen isotope fractionation equation of Mg-calcite (Friedman and O'Neil 1977): $1{,}000\ln\alpha=2.78(10^6/T^2)-2.89+0.06 \cdot$ mol% $MgCO_3$. Oxygen isotope fractionation equation of aragonite (Hudson and Anderson 1989):

   $$t=19.7-4.34\ [\delta^{18}O_{arag(PDB)}-\delta^{18}O_{H2O(SMOW)}]$$

References

Adams AE, MacKenzie WS, Guilford C (1986) Atlas der Sedimentgesteine in Dünnschliffen. Enke, Stuttgart, pp 1–103

Aharon P (1994) Geology and biology of modern and ancient submarine hydrocarbon seeps and vents: an introduction. Geo-Mar Lett 14:69–73

Bohrmann G, Greinert J, Suess E, Torres M (1998) Authigenic carbonates from the Cascadia subduction zone and their relation to gas hydrate stability. Geology 26:647–650

Boetius A, Ravenschlag K, Schubert CJ, Rickert D, Widdel F, Gieskes A, Amann R, Jørgensen BB, Witte U. Pfannkuche O (2000) A microbial consortium apparently mediating anaerobic oxidation of methane. Nature 407:623–626

Bruns TR, von Huene R, Culotta RC, Lewis SD, Ladd LW (1987) Geology and petroleum potential of the Shumagin margin Alaska. In: Scholl DW, Grantz A, Vedder JD (eds) Geology and resource potential of the continental margin of western North America and adjacent ocean basins – Beaufort to Baya California, vol 6. Houston Texas Circum-Pacific Council for Energy and Mineral Resources, Earth Science Series, pp 157–190

Burne RV, Moore LS (1987) Microbialites: organosedimentary deposits of benthic microbial communities. J Soc Sediment Geol Palaios 2:241–254

Creager JS, Scholl DW, Boyce RE, Echols RJ, Fullam TJ, Grow JA, Koizumi I, Lee HJ, Ling HY, Stewart RJ, Supko PR, Worsley TR (1973) Site reports. In: Supko PR (ed) Initial reports of the Deep Sea Drilling Project, Leg 19, University of California Scripps Institution of Oceanography, US Government Printing Office, Washington, pp 19–91

de Rosa M, Gambacorta A (1986) Lipid biosynthesis in archaebacteria. Syst Appl Microbiol 7:278–285

Duane MJ, Al-Zamel AZ (1999) Syngenetic textural evolution on modern sabkha stromatolites (Kuwait). Sediment Geol 127: 237–245

Elderfield H, Kastner M, Martin JB (1990) Composition and sources of fluids in the sediments of the Peru Subduction Zone. J Geophys Res 95:8819–8827

Elvert M, Suess E, Whiticar MJ (1999) Anaerobic methane oxidation associated with marine gas hydrates: superlight C-isotopes from saturated and unsaturated C_{20} and C_{25} irregular isoprenoids. Naturwissenschaften 86:295–300

Elvert M, Suess E, Greinert J, Whiticar MJ (2000) Archaea mediating anaerobic methane oxidation in deep-sea sediments at cold seeps of the eastern Aleutian subduction zone. Organ Geochem 31:1175–1187

Feldmann M, McKenzie JA (1998) Stromatolite–Thrombolite associations in a modern environment Lee Stocking Island Bahamas. J Soc Sediment Geol Palaios 13:201–212

Friedman I, O'Neil JR (1977) Compilation of stable isotope fractionation factors of geochemical interest. In: Fleischer M (ed) Data of geochemistry, 6th edn. US Geol Survey Professional Paper 440-KK

Fu B, Aharon P, Byerly GR, Roberts HH (1994) Barite chimneys on the Gulf of Mexico slope: initial report on their petrography and geochemistry. Geo-Mar Lett 14:81–87

Füchtbauer H (1988) Sedimente und Sedimentgesteine: Sediment-Petrologie, Teil II. Schweizerbart, Stuttgart, pp 1–1141

Gieskes JM, Lawrence JR (1981) Alteration of volcanic matter in deep-sea sediments. Evidence from the chemical composition of interstitial waters from deep-sea drilling cores. Geochim Cosmochim Acta 45:1687–1703

Greinert J (1999) Rezente submarine Mineralbildungen: Abbild geochemischer Prozesse an aktiven Fluidaustrittsstellen im Aleuten- und Cascadia-Akkretionskomplex. Dissertation Christian-Albrechts University Kiel, GEOMAR Report 87

Greinert J, Bohrmann G, Suess E (2001a) Gas hydrate-associated carbonates and methane-venting at Hydrate Ridge: classification distribution and origin of authigenic lithologies. In: Paull CK, Dillon PW (eds) Natural gas hydrates: occurrence, distribution, and dynamics. Geophys Monogr 124:99–113

Greinert J, Bollwerk SM, Derkachev A, Suess E, Obzhirov A, Sahling H, Tiedemann R, Bohrmann G (2001b) Barite and carbonate mineralization and cold fluid venting in the Derugin Basin, Sea of Okhotsk. Earth Planet Sci Lett (in review)

Grotzinger JG, Rothmann DH (1996) An abiotic model for stromatolitic morphogenesis. Nature 383:423–425

Hudson JC, Anderson TF (1989) Ocean temperatures and isotopic compositions through time. In: Clarkson ENK, Curry GB, Rolfe WDI (eds) Environments and physiology of fossil organisms. Trans R Soc Edinb 80:183–192

Iversen N, Jørgensen BB (1985) Anaerobic methane oxidation rates at the sulfate–methane transition in marine sediments from Kattegat and Skagerrak (Denmark). Limnol Oceanogr 30:944–955

Han MW, Suess E (1989) Subduction-induced pore fluid venting and the formation of authigenic carbonates along the Cascadia continental margin: implications for the global Ca-cycle. Palaeogeogr Palaeoclim Palaeoecol 71:97–118

Hoefs J (1987) Stable isotope geochemistry. Springer, Berlin Heidelberg New York

Hoehler TM, Alperin MJ, Albert DB, Martens CS (1994) Field and laboratory studies of methane oxidation in an anoxic marine sediment. Evidence for a methanogenic-sulfate reducer consortium. Global Biogeochem Cycles 8:451–463

Hofmann HJ (1973) Stromatolites characteristics and utility. Earth Sci Rev 9:339–373

Kastner M, Elderfield H, Martin JB (1991) Fluids in convergent margins: what do we know about their composition role in di-

agenesis and importance for oceanic chemical flux? In: Fluids in subduction zones. Philos Trans R Soc Lond Ser A:243–259
Kastner M, Sampel JC, Whiticar MJ, Hovland M, Cragg BA, Parkes JR (1995) Geochemical evidence for fluid flow and diagenesis at the Cascadia convergent margin. In: Carson B, Westbrook GK, Musgrave RJ, Suess E (eds) Proceedings of the Ocean Drilling Program, Scientific Results 146, part 1, pp 375–384
Kay RW, Sun SS, Lee-Hu CN (1978) Pb and Sr isotopes in volcanic rocks from the Aleutian Islands and Pribilof Islands Alaska. Geochim Cosmochim Acta 42:263–273
Kendall AC, Iannace A (2001) 'Sediment'–cement relationship in a Pleistocene speleothem from Italy: a possible analogue for 'replacement' cements and Archaeolithoporella in ancient reefs. Sedimentology 48:681–698
Kim ST, O'Neil JR (1997) Equilibrium and nonequilibrium oxygen isotope effects in synthetic carbonates. Geochim Cosmochim Acta 61:3461–3475
Knoll AH, Semikhatov MA (1998) The genesis and time distribution of two distinctive Proterozoic stromatolite microstructures. J Soc Sediment Geol Palaios 13:408–422
Kroopnick PM (1985) The distribution of ^{13}C of ΣCO_2 in the world oceans. Deep-Sea Res 32:57–84
Kulm LD, Suess E (1990) Relationship between carbonate deposits and fluid venting Oregon accretionary prism. J Geophys Res 95:8899–8915
Kulm LD, Suess E, Moore JC, Carson B, Lewis BT, Ritger SD, Kadko DC, Thornburg TM, Embley RW, Rugh WD, Massoth GJ, Langseth MG, Cochrane GR, Scamman RL (1986) Oregon subduction zone: venting fauna and carbonates. Science 231:561–566
Lewis SD, Ladd JW, Bruns TR (1988) Structural development of an accretionary prism by thrust and strike-slip faulting Shumagin region Aleutian trench. Geol Soc Am Bull 1000:767–782
Machel HG, Burton EA (1991) Factors governing cathodoluminescence in calcite and dolomite and their implication for studies of carbonate diagenesis, In: Barker CE, Kopp OC (eds) Luminescence microscopy quantitative and qualitative aspects. SEPM Short Course 25:37–57
Masuzawa T, Handa N, Kitagawa H, Kusakabe M (1992) Sulfate reduction using methane in sediments beneath a bathyal 'cold seep' giant clam community off Hatsushima Island Sagami Bay Japan. Earth Planet Sci Lett 110:39–50
Milliman JD (1974) Marine carbonates. Springer, Berlin Heidelberg New York
Moore JC, Vrolijk P (1992) Fluids in accretionary prisms. Rev Geophys 30:113–135
Nähr T, Stakes DS, Moore WS (2000) Mass wasting ephemeral fluid flow and barite deposits on the California continental margin. Geology 28:315–318
Neumann AC, Paull CK, Commeau RF, Commeau JA, Changon J, Martens CS, Trumbull W, Showers WJ (1988) Abyssal seep site cementation West Florida Escarpment. Am Assoc Petrol Geol Bull 72:228
Ostlund HG, Stuiver M (1980) Radiocarbon measurements on samples collected as part of the GEOSECS survey of the Pacific Ocean during the period September 1973 to June 1974. GEOSECS Pacific Radiocarbon 22:25–53
Pancost R, Sinninghe Damsté JS, de Lint S, van der Maarel MJEC, Gottschal JC, the *Medinaut* Shipboard Scientific Party (2000) Biomarker evidence for widespread anaerobic methane oxidation in Mediterranean sediments by a consortium of methanogenic archaea and bacteria. Appl Environ Microbiol 66:1126–1132
Paull CK, Chanton JP, Neumann AC, Coston JA, Martens CS (1992) Indicators of methane-derived carbonates and chemosynthetic organic carbon deposits: examples from the Florida escarpment. J Soc Sediment Geol Palaios 7:361–375
Paytan A, Kastner M, Martin EE, MacDougall JD, Herbert T (1993) Marine barite as a monitor of seawater strontium isotope composition. Nature 366:445–449
Rasmussen KA, Macintyre IG, Prufert L (1993) Modern stromatolite reefs fringing a brackish coastline Chetumal Bay Belize. Geology 21:199–202
Riding R (1991) Calcareous algae and stromatolites. Springer, Berlin Heidelberg New York
Ritger S, Carson B, Suess E (1987) Methane-derived authigenic carbonates formed by subduction-induced pore-water expulsion along the Oregon/Washington margin. Geol Soc Am Bull 98:147–156
Savard MM, Beauchamp B, Veizer J (1996) Significance of aragonite cements around cretaceous marine methane seeps. J Sediment Res 66:430–438
Southgate PN (1989) Relationship between cyclicity and stromatolite form in the late Proterozoic Bitter Springs Formation, Australia. Sedimentology 36:323–339
Suess E (1994) FS SONNE Fahrtbericht SO97 Kodiak-Vent. GEOMAR Report 29
Suess E, Bohrmann G (1997) RV SONNE Cruise Report SO 110 SO-RO. GEOMAR Report 59
Suess E, Whiticar MJ (1989) Methane-derived CO_2 in pore fluids expelled from the Oregon subduction zone. Palaeogeogr Palaeoclim Palaeoecol 71:119–136
Suess E, Bohrmann G, von Huene R, Linke P, Wallmann K, Lammers S, Sahling H, Winckler G, Lutz RA, Orange D (1998) Fluid venting in the eastern Aleutian subduction zone. J Geophys Res 103:2597–2614
Tarutani T, Clayton RN, Mayeda TK (1969) The effect of polymorphism and magnesium substitution on oxygen isotopic fractionation between calcium and water. Geochim Cosmochim Acta 33:987–996
Thiel V, Peckmann J, Seifert R, Wehrung P, Reitner J, Michaelis W (1999) Highly isotopically depleted isoprenoids: molecular markers for ancient methane venting. Geochim Cosmochim Acta 63:3959–3966
Visscher PT, Reid RP, Bebout BM, Hoeft SE, Macintyre IG, Thompson JA Jr (1998) Formation of lithified micritic laminae in modern marine stromatolites (Bahamas). The role of sulfur cycling. Am Mineral 83:1482–1493
von Huene R (1989) Continental margins around the Gulf of Alaska – the Geology of North America/the eastern Pacific and Hawaii. Geological Society of America Bulletin, Denver, pp 383–401
von Rad U, Rösch H, Berner U, Geyh M, Marchig V, Schulz H (1996) Authigenic carbonates derived from oxidized methane vented from the Makran accretionary prism off Pakistan. Mar Geol 136: 55–77
Wachter EA, Hayes JM (1985) Exchange of oxygen isotopes in carbon dioxide–phosphoric acid systems. Chem Geol 52:365–374
Walker G, Burley S (1991) Luminescence petrography and spectroscopy studies of diagenetic minerals, vol 25. In: Barker CE, Kopp OC (eds) Luminescence microscopy quantitative and qualitative aspects. SEPM Short Course, pp 83–96
Wallmann K, Linke P, Suess E, Bohrmann G, Sahlig H, Dählmann A, Lammers S, Greinert J, Mirbach NV (1997) Biogeochemical turnover and transport at cold vents of the Aleutian subduction zone. Geochim Cosmochim Acta 61:5209–5219
Wefer G, Berger WH (1991) Isotope paleontology growth and composition of extant calcareous species. Mar Geol 100: 201–248
Whiticar MJ (1996) Isotope tracking of microbial methane formation and oxidation. Mitt Int Verein Theor Angew Limnol 25: 39–54
Zhang Y, Lifang J, Shuhai X, Yuzuo L (1993) Image analysis of stromatolite fabric using a spatial frequency power spectrum analysis system. J Geol 101:591–602